Upconversion Dynamics in Er^{3+}-Doped Gd_2O_2S: Influence of Excitation Power, Er^{3+} Concentration, and Defects

*Rosa Martín-Rodríguez, Freddy T. Rabouw, Mattia Trevisani, Marco Bettinelli, and Andries Meijerink**

Upconversion (UC) enables the conversion of lower energy to higher energy photons and has gained interest for the application in solar cells and nanocrystal biolabels. Er^{3+}-doped Gd_2O_2S is a highly promising UC material for applications. A record UC quantum yield of 12% was recently measured in Gd_2O_2S doped with 10% Er^{3+} upon monochromatic excitation into the $^4I_{13/2}$ state at 1510 nm for moderate excitation densities (700 W m^{-2}). In this work, the focus is on the dynamics of the infrared ($^4I_{13/2}$, ≈1500 nm) to near-infrared ($^4I_{11/2}$, ≈1000 nm) UC luminescence in Er^{3+}-doped Gd_2O_2S. On the basis of luminescence spectra (emission and excitation), UC emission decay curves, and rate equation modeling, it is shown that energy transfer upconversion (ETU) is the mechanism responsible for the $^4I_{11/2}$ UC luminescence, and the ETU parameter for Gd_2O_2S:10%Er^{3+} is determined to be $W_{ETU} = 6.3 \times 10^{-19}$ cm^3 s^{-1}. The UC dynamics depend on the Er^{3+} concentration and, similar to triplet–triplet annihilation UC in organic materials, on the excitation power. The results highlight the subtle balance between desired energy transfer processes leading to ETU and undesired energy migration to quenching sites. The overall UC efficiency is dependent not only on the material and composition but also on the synthesis process.

1. Introduction

Upconversion (UC) processes in which two or more low-energy photons are combined to obtain one higher energy photon were discovered independently by Auzel[1] and Ovsyankin and Feofilov.[2] The study of UC materials has great importance for applications in different fields such as solid state lasers, bio-labeling, diagnostics, or efficiency enhancement of solar cells.[3–7] Particularly, for photovoltaic applications, an UC material located on the back side of a solar cell should efficiently convert transmitted sub-bandgap photons into high energy photons which can subsequently be absorbed by the solar cell. Er^{3+} is a promising ion to increase the efficiency of silicon solar cells (bandgap of 1.1 eV, 1100 nm) because excitation into the $^4I_{13/2}$ first excited state around 1500 nm gives rise to UC emission from higher excited states above the silicon bandgap.[8,9]

The most important UC processes are ground-state absorption followed by excited-state absorption (GSA/ESA) and energy transfer UC (GSA/ETU). The dominant mechanism can differ for continuous-wave and pulsed excitation. Typically, for broad-band continuous-wave excitation, ETU processes are two orders of magnitude more efficient than ESA mainly due to the fact that resonance is easily achieved and photons are able to interact for a longer time.[10] The most common way to distinguish between ESA and ETU processes is either from the UC excitation spectra (usually recorded for continuous-wave excitation) or the excited state dynamics (after pulsed excitation).[11] Different UC mechanisms have previously been proposed in the literature for the infrared to near-infrared Er^{3+} UC emission upon $^4I_{13/2}$ excitation. For instance, ETU was shown to be the dominant mechanism in Er^{3+}-doped $NaYF_4$ upon excitation at 1523 nm.[12] Chen et al. proposed different ETU processes based on power dependence experiments to describe the Er^{3+} UC emission upon 1490 nm excitation in $LiYF_4$:Er^{3+} nanocrystals.[13] However, although ETU is generally favored, Kumar et al. attributed the Er^{3+} UC emission upon 1550 nm excitation in Gd_2O_2S, Lu_2O_2S, and Y_2O_2S only to an ESA mechanism.[14]

A detailed spectroscopic study including temporal dependence of the UC luminescence is of great relevance for the understanding of the UC mechanisms. GSA/ESA involves one single ion, and since both GSA and ESA occur during the excitation pulse, the UC luminescence exhibits an immediate decay after pulsed excitation, with a lifetime identical to the one observed after direct excitation in the emitting state. In addition, since GSA and ESA steps occur at slightly different wavelengths, the GSA/ESA mechanism shows additional peaks in the UC excitation spectra, compared to the GSA spectrum. On the other hand, in the GSA/ETU mechanism, two ions excited by GSA to an intermediate level interact via nonradiative energy transfer to relax one ion to the ground state and promote the other ion to an upper state from where UC emission occurs.

Dr. R. Martín-Rodríguez, F. T. Rabouw, Prof. A. Meijerink
Department of Chemistry
Debye Institute for Nanomaterials Science
University of Utrecht
Princetonplein 5, 3584 CC Utrecht, The Netherlands
E-mail: A.Meijerink@uu.nl
Dr. M. Trevisani, Prof. M. Bettinelli
Department of Biotechnology
University of Verona
Strada Le Grazie 15, I-37134 Verona, Italy

DOI: 10.1002/adom.201400588

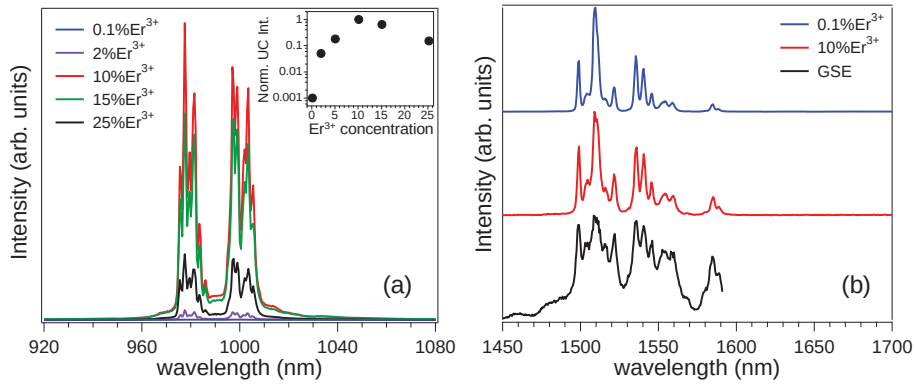

Figure 1. a) $^4I_{11/2}$ UC luminescence spectra of Gd_2O_2S doped with different Er^{3+} concentrations (0.1%, 2%, 10%, 15%, and 25%) upon excitation into the $^4I_{13/2}$ Er^{3+} level at 1510 nm. The inset shows the Er^{3+} concentration dependence of the integrated intensity in logarithmic scale. b) Excitation spectra of the $^4I_{11/2} \rightarrow {}^4I_{15/2}$ Er^{3+} UC luminescence, detecting 977.5 nm emission for the Gd_2O_2S microcrystals doped with 0.1% and 10%Er^{3+}, and GSE spectrum of Gd_2O_2S:10%Er^{3+} detecting 1595 nm emission.

This energy transfer step occurs after the pulse; hence, it is usually identified by a rise of the UC luminescence intensity after the excitation pulse. The rise time is strongly influenced by lifetime of the emitting state.[15] The ETU efficiency depends on the distance between the ions and the spectral overlap between the transitions involved.[16,17] Specifically, the efficiency of ETU and ESA processes scale quadratically and linearly, respectively, with the ion concentration. Based on the various differences between GSA/ESA and ETU outlined above, the dominant mechanism in an UC material can be established by careful spectroscopic studies including time resolved, concentration, and power dependent measurements.

Here we investigate the dynamics and the high quantum yield of the infrared to near-infrared UC luminescence in Gd_2O_2S:Er^{3+}. The dominant mechanisms depend on Er^{3+} concentration and excitation conditions. We study a series of Er^{3+}-doped Gd_2O_2S microcrystalline samples with different dopant concentrations (0.1%, 2%, 10%, 15%, and 25%, in mol% substituting Gd^{3+}). We compare this UC material with the well-known UC material $NaYF_4$ doped with 25%Er^{3+}, which is the optimum doping concentration for this system.[18] $NaYF_4$:Er^{3+} is a standard UC material and was obtained from K.W. Krämer group, where the most efficient $NaYF_4$ UC materials are produced. We focus on the $^4I_{9/2}$ and $^4I_{11/2}$ near-infrared UC luminescence, although UC emission from higher Er^{3+} excited states ($^4I_{9/2}$, $^4F_{9/2}$, and $^4S_{3/2}$ –$^2H_{11/2}$) is also observed. The $^4I_{11/2}$ UC emission at 990 nm dominates and represents ≈97% of the total UC luminescence intensity. This is mostly due to the fact that $^4I_{9/2}$ and $^4I_{11/2}$ UC luminescence is a two-photon process, while at least three photons are involved in the red $^4F_{9/2}$ and green $^4S_{3/2}$ UC emissions.[19] We measured the $^4I_{9/2}$ and $^4I_{11/2}$ UC luminescence decay curves upon pulsed excitation into the maximum of the $^4I_{13/2}$ excitation band at 1510 nm, and investigated the excited state dynamics by a simple rate equation model. Our results provide insight in the underlying physical mechanisms responsible for the efficient UC luminescence.

A second focus in this work is the influence of the excitation power on the UC emission dynamics. The dependence of the UC luminescence *intensity* on the excitation power has been extensively investigated in many UC materials and was previously described by using a rate equation model.[20,21] In addition, there are several models in the literature describing the nature of the UC excitation process, and the influence of energy transfer, energy migration and quenching processes on the UC mechanisms, as summarized by Pollnau *et al.*[17] However, the excitation power dependence of the UC emission dynamics has not been experimentally studied yet, and in this work we show that the variation of the excitation power leads to interesting changes in the UC decay curves. We focus on the excitation power dependence of the $^4I_{9/2}$ and $^4I_{11/2}$ UC emission lifetime in order to validate the mechanism proposed for the near-infrared UC luminescence in Er^{3+}-doped Gd_2O_2S and to further clarify the high UC quantum yield observed in Gd_2O_2S:Er^{3+}. We demonstrate that the $^4I_{11/2}$ UC rise time decreases when increasing the excitation power. This behavior has been previously observed and discussed in the UC emission in organic molecules based on triplet–triplet annihilation.[22,23] We also discuss the dependence of the UC dynamics on the Er^{3+} concentration, as well as the influence of energy migration, reabsorption, and concentration quenching. Finally, the influence of unintentional quenching centers on the performance and quantum yield of the UC material is investigated, revealing that a high UC efficiency is not only a material property but also requires optimization of the synthesis conditions.

2. Results and Discussion

2.1. UC Mechanism in Er^{3+}-Doped Gd_2O_2S

In this section we identify the dominant UC mechanism in Er^{3+}-doped Gd_2O_2S by studying UC luminescence and excitation spectra as well as decay curves which are analyzed by rate equations to model the observed decay dynamics. **Figure 1**a shows the UC luminescence spectra in the near-infrared region of Gd_2O_2S microcrystalline samples doped with different Er^{3+} concentrations. The emission peaks centered at 990 nm are assigned to the $^4I_{11/2} \rightarrow {}^4I_{15/2}$ transition of Er^{3+} ions. The inset in Figure 1a shows the Er^{3+} concentration dependence of the $^4I_{11/2}$

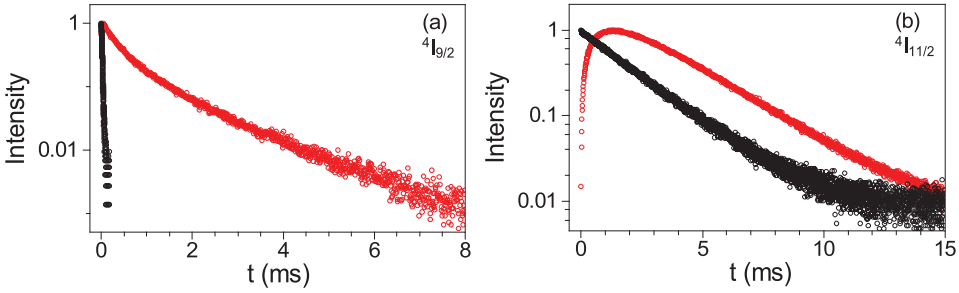

Figure 2. Temporal dependence of the Er^{3+} emission intensity from the a) $^4I_{9/2}$ and b) $^4I_{11/2}$ excited states after pulsed excitation at 1510 nm (red, UC emission), and upon direct excitation (black), at 800 nm and 975 nm, respectively, in Gd_2O_2S:10%Er^{3+} (logarithmic scale).

UC emission integrated intensity. It is clear that that Gd_2O_2S doped with 10%Er^{3+} is the most efficient sample for the excitation power used (10^6 W cm^{-2} during the ≈10 ns pulse). The integrated intensity depends supralinearly on Er^{3+} concentration below the optimum concentration (10%). In particular, the UC luminescence intensity in Gd_2O_2S:10%Er^{3+} is ≈1000 times higher than in Gd_2O_2S:0.1%Er^{3+}. The fact that the UC emission intensity is not linearly dependent on the Er^{3+} concentration suggests that Er^{3+} UC emission in Gd_2O_2S is not a single ion process (as expected for GSA/ESA), it is rather associated with the probability of forming Er^{3+} pairs showing ETU UC. The fact that the quadratic dependence corresponding to a pure ETU process is not observed either is ascribed to the influence of energy migration and concentration quenching effects at higher concentrations.

Figure 1b shows the excitation spectra of the $^4I_{11/2} \rightarrow ^4I_{15/2}$ Er^{3+} UC luminescence at 977 nm in the $^4I_{15/2} \rightarrow ^4I_{13/2}$ region for Gd_2O_2S doped with 0.1% and 10% Er^{3+}. The ground-state excitation (GSE) spectrum of Gd_2O_2S:10%Er^{3+} for $^4I_{13/2}$ emission at 1595 nm is shown for comparison. As expected for the ETU mechanism, the UC excitation spectrum is narrower than the GSE spectrum, with no additional features. This indicates that the $^4I_{13/2} \rightarrow ^4I_{9/2}$ ESA contribution is negligible and the ETU mechanism is dominant for the 10% Er^{3+}-doped Gd_2O_2S, and even for the low-concentrated sample doped with 0.1% Er^{3+}.[24]

Next, we compare the excited state dynamics upon direct ($^4I_{9/2}$ or $^4I_{11/2}$) and UC ($^4I_{13/2}$) excitation in Gd_2O_2S:10%Er^{3+}. **Figure 2** shows the emission decay curves of the (a) $^4I_{9/2}$ state and (b) $^4I_{11/2}$ state, upon direct pulsed excitation into the emitting states. The decay curves are nearly single exponential with lifetimes of 17.5 ± 0.5 µs for the $^4I_{9/2}$ state and 2.0 ± 0.1 ms for the $^4I_{11/2}$ state. A lifetime of 2.8 ± 0.1 ms was measured for the $^4I_{13/2}$ state (excitation at 1510 nm and detection at 1560 nm, data not shown). The decay times obtained upon direct excitation (direct lifetimes) provide valuable information to properly correlate the UC decay curves with the UC mechanism. We also show the dynamics of the $^4I_{9/2}$ and $^4I_{11/2}$ UC emission upon excitation at 1510 nm, when the emitting states are populated via the $^4I_{13/2}$ state. The UC decay curves are markedly different from those measured for direct excitation. The UC decay of the $^4I_{9/2}$ emission (Figure 2a, red) is two orders of magnitude slower than upon direct excitation (Figure 2a, black). This is a clear fingerprint of ETU, where the UC emission is observed as long as the long-lived $^4I_{13/2}$ intermediate state remains populated. In the $^4I_{11/2}$ UC luminescence decay (Figure 2b, red) a slow rise is clearly detected before the decay. The rise of the UC emission intensity after the excitation pulse is another clear signature for ETU mechanism. An analogous behavior for the $^4I_{9/2}$ and $^4I_{11/2}$ UC emission decay curves is observed for other Er^{3+} concentrations, including 0.1% (see Section 2.3). As we discussed in a previous paper, both $^4I_{15/2} \rightarrow ^4I_{13/2} \rightarrow ^4I_{11/2}$ ESA and ($^4I_{13/2}$, $^4I_{13/2}$) → ($^4I_{15/2}$, $^4I_{11/2}$) ETU mechanisms can be ruled out, due to the large energy mismatch (around 3000 cm^{-1}) and the low maximum phonon energy in Gd_2O_2S (440 cm^{-1}).[19]

Based on the above results on emission, excitation, and dynamics, we conclude that UC in Gd_2O_2S:10%Er^{3+} occurs via the GSA/ETU mechanism depicted in **Figure 3**. After excitation of two Er^{3+} ions into the $^4I_{13/2}$ level at 1510 nm, the ($^4I_{13/2}$, $^4I_{13/2}$) → ($^4I_{15/2}$, $^4I_{9/2}$) ETU process promotes one Er^{3+} ion to the $^4I_{9/2}$ state. Radiative decay from this level to the $^4I_{15/2}$ ground state gives UC emission centered at 820 nm (blue arrow). Alternatively, considering the small energy gap between the $^4I_{9/2}$ and $^4I_{11/2}$ levels (≈2000 cm^{-1}), efficient $^4I_{9/2} \rightarrow ^4I_{11/2}$ multiphonon relaxation followed by radiative decay of the $^4I_{11/2}$ state gives rise to the most intense UC emission at 990 nm (red arrow).

Interestingly, the $^4I_{9/2}$ UC decay curve exhibits an almost immediate decay, while the time dependence of the $^4I_{11/2}$ UC emission displays a slow rise (Figure 2), although both emitting levels are populated by the same ETU process. This observation seems surprising but we can explain it in terms of the arguments developed by Gamelin and Güdel to understand the UC luminescence dynamics.[15] Using a simple rate equation model on a three-level system (ground-state, intermediate-state and emitting-state), they showed that if the lifetime of the intermediate state is longer than the lifetime of the emitting state, the rise of the UC lifetime is strongly influenced by the lifetime of the emitting state in an ETU process.[15] Therefore, since the lifetime of the $^4I_{13/2}$ intermediate level is longer than both $^4I_{9/2}$ and $^4I_{11/2}$ lifetimes, the fast rise observed in the temporal dependence of the $^4I_{9/2}$ UC emission correlates with the short lifetime of the $^4I_{9/2}$ state (17.5 µs), while the slow rise of

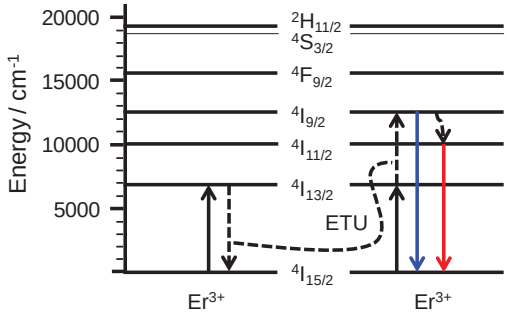

Figure 3. Energy level diagram of Er^{3+} ions and the proposed mechanisms giving rise to the $^4I_{9/2}$ and $^4I_{11/2}$ UC luminescence.

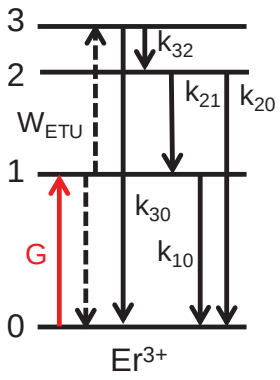

Figure 4. Diagram of the four-level system and ETU process responsible for the infrared Er^{3+} UC emissions. The levels 0, 1, 2, and 3 represent the $^4I_{15/2}$, $^4I_{13/2}$, $^4I_{11/2}$, and $^4I_{9/2}$ level, respectively.

the $^4I_{11/2}$ UC luminescence intensity after the excitation pulse is related to the much longer lifetime of the $^4I_{11/2}$ level (2.0 ms).

To further analyze the UC mechanism proposed, we introduce the four-level system shown in **Figure 4**. States 0, 1, 2, and 3 in the model correspond to the $^4I_{15/2}$, $^4I_{13/2}$, $^4I_{11/2}$, and $^4I_{9/2}$ states of the Er^{3+} ion (Figure 3), respectively. A short laser pulse generates an initial population at $t = 0$ in state 1, N_{10}. Subsequently, considering the previously described ETU mechanism (see Figure 3), the system evolves according to the following rate equations:

$$\begin{aligned}
\frac{dn_0}{dt} &= k_{10}n_1 + k_{20}n_2 + k_{30}n_3 + W_{ETU}N_1n_1 \\
\frac{dn_1}{dt} &= -k_{10}n_1 - 2W_{ETU}N_1n_1 + k_{21}n_2 \\
\frac{dn_2}{dt} &= -(k_{21} + k_{20})n_2 + k_{32}n_3 \\
\frac{dn_3}{dt} &= -(k_{32} + k_{30})n_3 + W_{ETU}N_1n_1
\end{aligned} \quad (1)$$

Both n_i and N_i are time dependent, n_i is the fraction of Er^{3+} ions in the state i, while N_i is the Er^{3+} population density for the state i in units of cm^{-3} according to $N_i = n_i\phi N$, where ϕ is the Er^{3+} concentration in the sample (percentage of cation sites) and N is the cation site number density in the host material (in units of cm^{-3}). k_{if} represents the transition probability between two states, i to f. From our measurements of luminescence lifetimes after direct excitation we know that $k_{10} = 1/\tau(^4I_{13/2})$, $k_{21} + k_{20} = 1/\tau(^4I_{11/2})$ and $k_{32} + k_{30} = 1/\tau(^4I_{9/2})$. The energy transfer process is controlled by the product $W_{ETU}N_1$, W_{ETU} being the average power-independent energy transfer parameter.[15,17] For simplicity, additional processes such as cross relaxation between excited states or transfer to defects in the host-lattice are not considered in this model.

The interpretation of the average energy transfer parameter, W_{ETU}, in our simple model is not straightforward. Considering dipole–dipole interaction, each individual Er^{3+}–Er^{3+} pair has an energy transfer parameter proportional to R^{-6}, R being the cation–cation separation.[25] For a high Er^{3+} concentration in the sample, fast energy migration ensures that W_{ETU} is the simple average over all possible Er^{3+}–Er^{3+} pairs. At low Er^{3+} concentration, on the other hand, energy migration hardly occurs. As a result, only those few close-neighbors Er^{3+}–Er^{3+} pairs which show UC contribute to the apparent average W_{ETU}. As we will show later, for the Er^{3+} concentrations studied in this work, energy migration is fast enough to work with a W_{ETU} averaged over all possible Er^{3+}–Er^{3+} pairs, except for the lowest concentration (0.1%). The concentration and excitation power dependence of the energy transfer rate, $W_{ETU}N_1$, are then both contained in the initial population of state 1, N_{10}.

Figure 5 displays the $^4I_{11/2}$ and $^4I_{9/2}$ UC luminescence decay curves (red and blue dots) in Gd_2O_2S:10%Er^{3+}, and the simulated N_2 and N_3 dynamics (black lines) calculated for an ETU process (Equation (1)), after high-power excitation at 10^6 W cm^{-2}. For the simulation of N_2 (Figure 5a), the values for k_{if} were fixed, and the initial energy transfer rate, $W_{ETU}N_{10}$, was the only free parameter. Particularly, the transition probabilities are known from the experimentally measured lifetimes of the levels involved in Gd_2O_2S:10%Er^{3+}: $k_{10} = 1/\tau(^4I_{13/2}) = 400$ s^{-1}, $k_{21}+k_{20} = 1/\tau(^4I_{11/2}) = 500$ s^{-1} and $k_{32} + k_{30} = 1/\tau(^4I_{9/2}) = 57150$ s^{-1}. The radiative and nonradiative decay components for the $^4I_{9/2}$ and $^4I_{11/2}$ states were estimated as follows: The fact that the $^4I_{11/2}$ emission represents 97% of the total UC emission at this excitation power[19] signifies fast multiphonon relaxation from the $^4I_{9/2}$ to the $^4I_{11/2}$ level. Thus, the ratio of the $^4I_{9/2}$ radiative and nonradiative decay probabilities, k_{30}:k_{32}, is ≈3:100. In addition, since the $^4I_{11/2}$ –$^4I_{13/2}$ energy gap is ≈3500 cm^{-1}, which corresponds to 8 phonons, the $^4I_{11/2}$ decay rate is mainly radiative. The best fitting of the $^4I_{11/2}$ UC emission lifetime to Equation (1) provides an energy transfer rate of $W_{ETU}N_{10}$ = 740 s^{-1} (see inset in Figure 5a). For the simulated N_3 curve ($^4I_{9/2}$

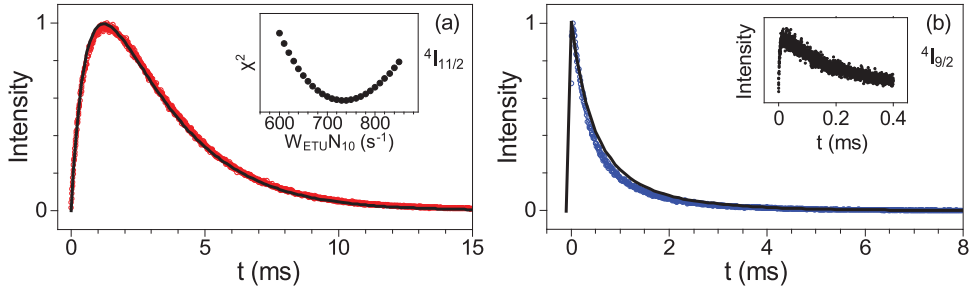

Figure 5. Experimentally observed decay curves of the a) $^4I_{11/2}$ (red) and b) $^4I_{9/2}$ (blue) UC luminescence, and dynamics of the a) N_2 and b) N_3 (black lines) excited-states populations, after excitation with a ns pulse into the intermediate state (level 1), based on the rate equation model (Equation (1)) (see text). Inset in a) shows the chi-square values obtained upon comparison of the experimental $^4I_{11/2}$ UC decay curve with the N_2 fitting derived for different $W_{ETU}N_{10}$ values. Inset in b) displays a zoom-in of the $^4I_{9/2}$ fast rise after the excitation pulse.

decay) all parameters k_{if} and $W_{ETU}N_{10}$ were fixed, and as can be seen in Figure 5b, the simulated decay curve is in good agreement with the experimental $^4I_{9/2}$ UC emission decay curve. Importantly, a slow rise is observed for the N_2 decay curve while the N_3 time dependence shows a faster decay after the excitation pulse (note the fast rise in inset in Figure 5b), being $k_{21} + k_{20} \gg k_{32} + k_{30}$ ($\tau(^4I_{11/2}) \gg \tau(^4I_{9/2})$). Thus, the N_2 and N_3 decay curves corroborate earlier results showing that the UC rise time strongly depends on the lifetime of the emitting state.[15]

2.2. Influence of the Excitation Power on the UC Dynamics

In this section, we analyze the influence of the excitation power on the UC dynamics in Er^{3+}-doped Gd_2O_2S upon excitation into the $^4I_{13/2}$ level. We model the results by using the rate equation model presented in the previous section (Equation (1)). According to the rate equation model, the initial population N_{10} of the $^4I_{13/2}$ intermediate state is the key parameter determining the UC dynamics, since the energy transfer process is governed by the product $W_{ETU}N_1$. The N_{10} initial population, in turn, is set by the $^4I_{15/2} \rightarrow {}^4I_{13/2}$ absorption oscillator strength and the excitation power density. From our results at high excitation power, we are able to estimate the power-independent energy transfer parameter, W_{ETU}.

Figure 6a,b shows the excitation power dependence of the $^4I_{9/2}$ and $^4I_{11/2}$ UC luminescence decay curves in Gd_2O_2S:10%Er^{3+}. When the excitation power increases the $^4I_{9/2}$ UC dynamics become faster and more nonexponential. A

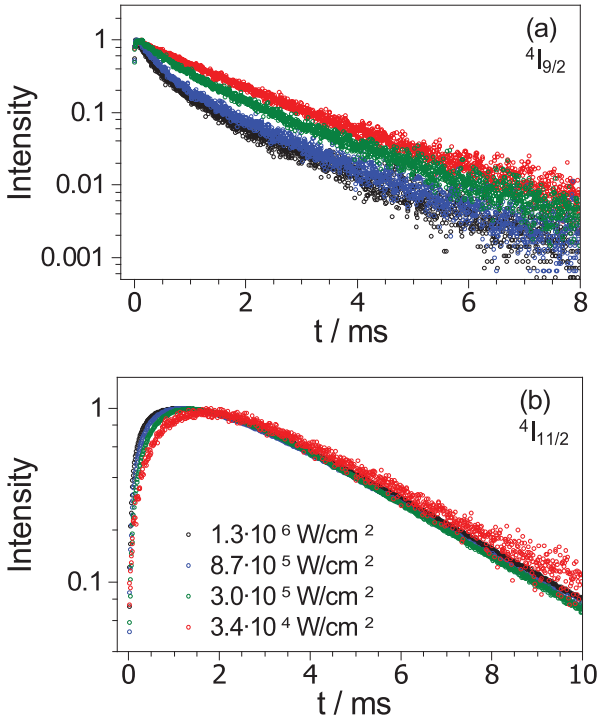

Figure 6. Decay curves of the Er^{3+} UC luminescence from the a) $^4I_{9/2}$ and b) $^4I_{11/2}$ excited states in Gd_2O_2S:10%Er^{3+} for different excitation powers at 1510 nm.

similar behavior was previously observed in the time dependence of the UC emission in Mo^{3+}-doped Cs_2NaYBr_6[25] and Nd^{3+}-doped $LiYF_4$.[26] The $^4I_{9/2}$ UC emission shows a very fast rise regardless of the excitation power. In contrast, the rise time of the $^4I_{11/2}$ UC emission becomes clearly shorter for higher excitation power. This feature is consistent with the fact that, for higher excitation power, the number of Er^{3+} ions in the $^4I_{13/2}$ intermediate state, N_{10}, is larger (see Figure 4 and Equation (1), and the probability of the ($^4I_{13/2}$, $^4I_{13/2}$) $\rightarrow$ ($^4I_{15/2}$, $^4I_{9/2}$) ETU process increases.[17] The influence of the excitation power on the $^4I_{11/2}$ UC luminescence *decay* time, on the other hand, is small. For a more quantitative comparison of the UC dynamics as a function of excitation power, we fitted the $^4I_{9/2}$ UC emission decay curves to a single-exponential at low excitation power, and to a biexponential decay at higher excitation powers. Besides, the temporal evolution of the $^4I_{11/2}$ UC luminescence was fitted to a Vial's type equation, where τ_D and τ_R represents the decay and rise of the transient, respectively:[27]

$$I(t) = Ae^{-t/\tau_D} - Be^{-t/\tau_R} \quad (2)$$

Figure 7a presents the excitation power dependence of the $^4I_{9/2}$ UC decay time in Gd_2O_2S:10%Er^{3+}. Figure 7b,c shows the power dependence for the rise and decay time of the $^4I_{11/2}$ UC emission in Gd_2O_2S:10%Er^{3+}. The excitation power dependence of the $^4I_{11/2}$ UC luminescence *intensity* in Gd_2O_2S:10%Er^{3+} determined from emission spectra is also depicted (Figure 7d). The faster $^4I_{9/2}$ UC decay (Figure 7a) and $^4I_{11/2}$ UC rise (Figure 7b) at higher excitation power are explained in terms of the rate equation model. Higher excitation powers lead to a larger initial population N_{10} in the $^4I_{13/2}$ intermediate level, which in turns results in a faster ETU. The population of the $^4I_{13/2}$ intermediate level reveals the influence of the excitation power on the $^4I_{11/2}$ and $^4I_{9/2}$ dynamics, represented by the N_2 and N_3 populations (Figure 4). On the contrary, the lengthening of the $^4I_{11/2}$ UC decay (Figure 7c) cannot be understood from our simple rate equation modeling. The simulations show no change in the decay time with increasing excitation power, and the origin of this observation is unclear.

It is generally affirmed in the literature that the UC intensity in a two-photon process follows a quadratic power dependence ($\log(I) \doteq 2\log(P)$, slope two). However, this is only true at low-power excitation, and Gamelin and Gudel amongst others, demonstrated that the slope decreases when increasing the excitation power.[15] A slope of one is expected in the high-power limit for a two-photon ETU process.[21] In addition, the temporal evolution of the UC emission is also power dependent. Under low-power excitation the rise and decay times are expected to be independent of the excitation power. On the contrary, under high-power conditions, both $^4I_{11/2}$ and $^4I_{9/2}$ decay curves depend on the $^4I_{13/2}$ population, which is linearly proportional to the excitation power.[15] Thus, it is clear from the results of Figure 7 that our experiments are performed at high-power excitation . To prove this assumption we measured the power dependence of the $^4I_{11/2}$ UC emission *intensity* in the same power range as the UC decay curves. Figure 7d displays the $^4I_{11/2}$ UC luminescence intensity versus the excitation power density at 1510 nm for Gd_2O_2S:10%Er^{3+} and a slope of 1.3 was obtained. This reduction of the slope confirms that our

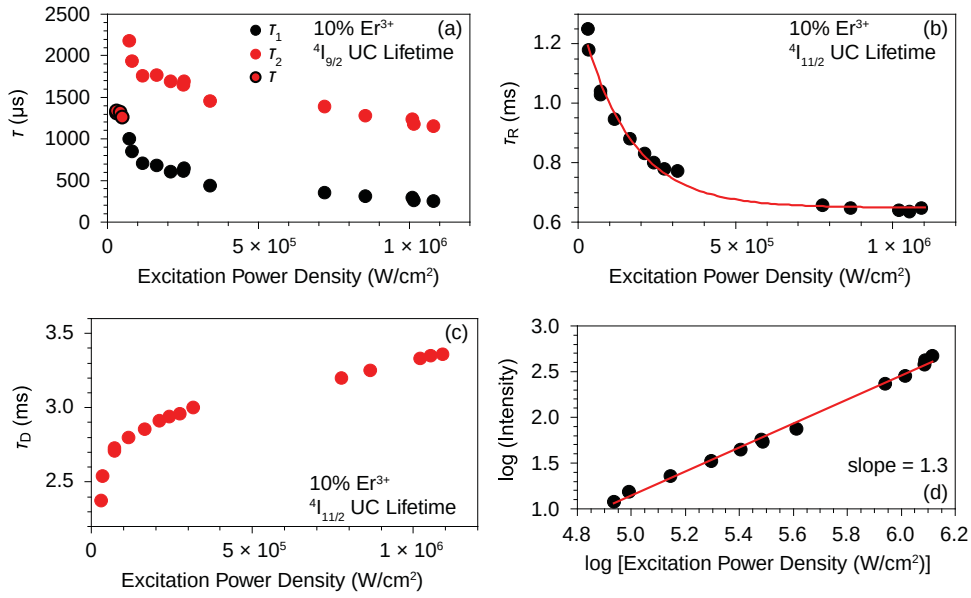

Figure 7. a) $^4I_{9/2}$ UC emission lifetime in Gd_2O_2S:10%Er^{3+} for different excitation power density considering either single- or biexponential decay. Excitation power dependence of the b) $^4I_{11/2}$ UC luminescence rise time and c) decay time in Gd_2O_2S:10%Er^{3+}, determined from fits to a Vial's type equation (Equation). d) Excitation power dependence of the $^4I_{11/2}$ UC emission intensity in Gd_2O_2S:10%Er^{3+}.

experimental conditions correspond to a high-power regime which is not unexpected given the high power density (≈10^5 W cm^{-2}) during the excitation pulses.

Inspection of Figure 7b indicates that the $^4I_{11/2}$ UC rise time in Gd_2O_2S:10%Er^{3+} becomes shorter with increasing excitation power and reaches an asymptotic value in the high-power limit (above 7 × 10^5 W cm^{-2}). This represents saturation of the initial GSA (i.e., n_1 approaches 0.5), leading to a maximum of the subsequent ($^4I_{13/2}$, $^4I_{13/2}$) → ($^4I_{15/2}$, $^4I_{9/2}$) ETU rate. The corresponding limit value for the rise time is ≈650 μs. To estimate the energy transfer parameter, W_{ETU}, the $W_{ETU}N_{10}$ values at different excitation powers were obtained by fitting the $^4I_{11/2}$ UC emission decay curves in Gd_2O_2S:10%Er^{3+} to the rate equation model described in Section 2.1 (Equation (1) and Figure 4). All decay constants k_{if} were kept fixed, so that the product $W_{ETU}N_{10}$ was the only free parameter. As described in the previous section, $k_{10} = 1/\tau(^4I_{13/2}) = 400\ s^{-1}$, $k_{21}+k_{20} = 1/\tau(^4I_{11/2}) = 500\ s^{-1}$, and $k_{32}+k_{30} = 1/\tau(^4I_{9/2}) = 57\,150\ s^{-1}$.

Figure 8 shows the initial energy transfer rate, i.e., the product of the ETU parameter and the initial $^4I_{13/2}$ intermediate population, $W_{ETU}N_{10}$, versus the excitation power in Gd_2O_2S:10%Er^{3+}. Analogously to the rise time, τ_R, behavior (Figure 7b), $W_{ETU}N_{10}$ increases with the excitation power and reaches an stationary limit. If N_{10} is known, the power-independent ETU parameter, W_{ETU}, can be determined.[28,29] The initial population N_{10} can be derived from

$$\frac{dN_1}{dt} = PN_0 - PN_1 - k_{10}N_1 = PN_{tot} - (k_{10}+2P)N_1 = 0 \quad (3)$$

where $N_0 = N_{tot} - N_1$. Thus, we fitted the excitation power dependence of the obtained $W_{ETU}N_{10}$ values to the following equation, W_{ETU} and A being the fit parameters:

$$W_{ETU}N_{10} = W_{ETU}\frac{AP}{k_{10}+2AP}\phi N_{tot} \quad (4)$$

$\phi N_{tot} = 2.3\times10^{21}\,cm^{-3}$ is the total density of Er^{3+} ions in the crystal (from the density of 7.34 g cm^{-3} of Gd_2O_2S and the 10% Er^{3+} doping). The fraction of Er^{3+} ions excited by the laser pulse, $AP/(k_{10}+2AP)$, is determined by the interplay between spontaneous emission rate, $k_{10} = 1/\tau(^4I_{13/2}) = 400\ s^{-1}$, and absorption and stimulated emission rates, both scaling linearly with the excitation power P. The prefactor A in the absorption and stimulated emission rate depends on the cross-section of the transition. We neglect the difference in degeneracy between the ground and intermediate state. Equation (4) describes how in the high-power limit ($AP \gg k_{10}$) the maximum initial population of the intermediate level is reached with half of the Er^{3+} ions excited to the $^4I_{13/2}$ state: $n_{10} = 1/2$ and $N_{10} = \frac{1}{2}\phi N$. Fitting the experimental data points of Figure 8 to Equation (4) yields

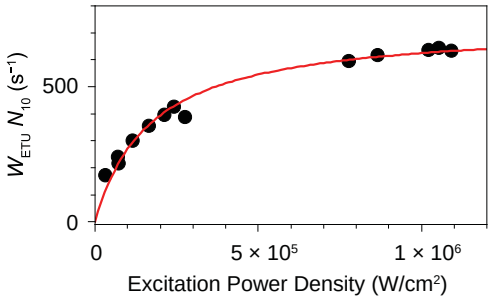

Figure 8. Values for $W_{ETU}N_{10}$ determined from fitting the experimental $^4I_{11/2}$ UC decay curves to the rate equation model, as a function of the excitation power density. The red solid line represents the fit of the experimental data to Equation (3) (see text).

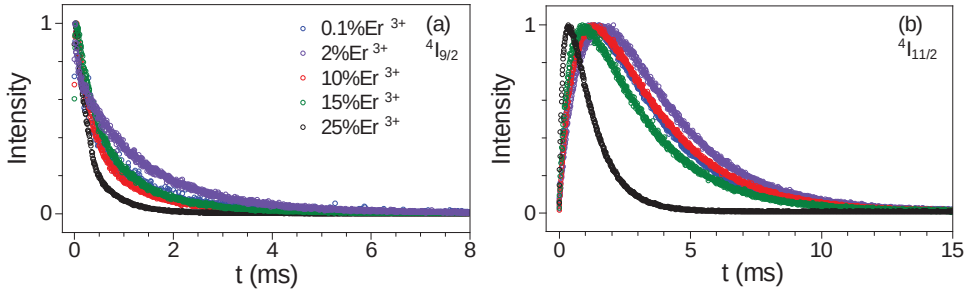

Figure 9. Temporal evolution of the Er^{3+} UC emission from the a) $^4I_{9/2}$ and b) $^4I_{11/2}$ excited states in Er^{3+}-doped Gd_2O_2S for different Er^{3+} concentrations, upon pulsed excitation at 1510 nm.

$W_{ETU} = 6.3 \times 10^{-19}$ cm^3 s^{-1}. This energy transfer parameter is one order of magnitude smaller than the one for Er^{3+}-doped $Y_3Al_5O_{12}$,[30] and three orders of magnitude smaller than the values measured for Nd^{3+}-doped $LiYF_4$ and $Y_3Al_5O_{12}$ by Pollnau *et al.*[29] and Guyot *et al.*,[26] respectively, in accordance with the higher oscillator strength in Nd^{3+}.

We demonstrated in a previous paper[19] an internal UC quantum yield of 12% ± 1% for Gd_2O_2S:10%Er^{3+} under continuous-wave excitation into the $^4I_{13/2}$ state at 700 Wm^{-2}. This is the highest value reported so far and is significantly higher than the 8.9% ± 0.7% quantum yield measured for $NaYF_4$:25%Er^{3+} (the optimum Er^{3+} concentration in $NaYF_4$) at the same excitation power density.[19] We aim to understand the high UC efficiency of Er^{3+}-doped Gd_2O_2S compared to Er^{3+}-doped $NaYF_4$, under monochromatic excitation. Therefore, we also simulated the $^4I_{11/2}$ UC emission decay curves at different excitation powers for $NaYF_4$:25%Er^{3+} (data not shown), considering the ($^4I_{13/2}$, $^4I_{13/2}$) → ($^4I_{15/2}$, $^4I_{9/2}$) ETU mechanism (Equation (1) and Figure 4). We performed the same analysis and the energy transfer parameter obtained from the UC emission decay curves at high-power is one order of magnitude smaller ($W_{ETU} = 8.0 \times 10^{-20}$ cm^3 s^{-1}). Thus, the comparison of the power-dependent UC dynamics for Er^{3+} in Gd_2O_2S and $NaYF_4$ reveals a higher energy transfer rate between Er^{3+} ions in Gd_2O_2S. This is consistent with higher oscillator strengths for Er^{3+} in Gd_2O_2S compared to $NaYF_4$, since while the radiative rates k_{if} scale linearly with the transitions strengths, the ETU parameter scales quadratically.[19] The higher UC energy transfer rate can give rise to more efficient UC. However, a stronger difference between the UC quantum yield in Er^{3+}-doped Gd_2O_2S and $NaYF_4$ would be expected if the energy transfer parameter, W_{ETU}, was the only parameter involved. As we will show in the following section, apart from W_{ETU}, which is an intrinsic property of the host material, the most important factor contributing to the high UC quantum yield of Er^{3+}-doped Gd_2O_2S is the absence of quenching processes, and the final UC efficiency depends on a balance between UC energy transfer processes and processes giving rise to infrared emission or quenching by defects.

2.3. Er^{3+} Concentration Dependence of the UC Dynamics

To gain further understanding of the UC processes, the dependence of the UC luminescence dynamics in Er^{3+}-doped Gd_2O_2S is investigated for different Er^{3+} concentrations ([Er^{3+}]). To allow for a meaningful comparison of the results, throughout this section the excitation power density is fixed at 1.2×10^5 W cm^{-2}. The results show how processes such as energy migration, reabsorption and concentration quenching complicate the interpretation of experimental data on UC dynamics. **Figure 9** presents the Er^{3+} concentration dependence of the $^4I_{9/2}$ and $^4I_{11/2}$ Er^{3+} UC dynamics in Gd_2O_2S. The decay curves of the $^4I_{11/2}$ Er^{3+} UC emission were fitted to a Vial's type equation (Equation (2)) and the obtained rise and decay times are collected in **Table 1**.

The rise time is considerably longer in Gd_2O_2S:2%Er^{3+} compared to the very dilute sample doped with 0.1%Er^{3+}. Gd_2O_2S samples doped with 0.1% Er^{3+} and 10% Er^{3+} show the same rise time within the experimental error and a substantial decrease of the rise time is observed above 10% Er^{3+}. These experimental results can be accounted for as follows: In Gd_2O_2S:0.1%Er^{3+} only energy transfer between closest Er^{3+} neighbors forming pairs is expected to occur and energy migration can be neglected. However, the energy migration probability increases when Er^{3+} concentration increases. Thus, energy migration among Er^{3+} ions prior to the ETU process can explain the slower rise time observed for Gd_2O_2S:2%Er^{3+} and demonstrates the importance of energy migration at this intermediate concentration. Additionally, the drop of the rise time as the Er^{3+} concentration increases beyond 2% can be ascribed to the combined effect of faster energy migration and especially a higher initial population of the $^4I_{13/2}$ intermediate state. Due to the higher initial population of Er^{3+} ions in the $^4I_{13/2}$ excited state, most Er^{3+} ions have a nearby excited Er^{3+} ion giving rise to a fast UC without energy migration.

We simulated the $^4I_{11/2}$ UC emission decay curves for different Er^{3+} concentrations, for the ($^4I_{13/2}$, $^4I_{13/2}$) → ($^4I_{15/2}$, $^4I_{9/2}$) ETU mechanism and the four-level system previously described (Equation (1) and Figure 4). We assumed fixed values

Table 1. Decay and rise times of the $^4I_{11/2}$ UC emission using a Vial's type model (Equation (2) in Gd_2O_2S samples doped with different Er^{3+} concentrations, [Er^{3+}], under pulsed excitation at 1510 nm (from fits to the results presented in Figure 9b).

[Er^{3+}]	τ_D [ms]	τ_R [μs]
0.1%	2.50 ± 0.05	820 ± 20
2%	2.55 ± 0.05	1190 ± 20
10%	2.80 ± 0.05	840 ± 20
15%	2.50 ± 0.05	490 ± 20
25%	1.15 ± 0.05	195 ± 20

Table 2. $W_{ETU}N_{10}$ values in the ETU mechanism responsible for the UC emission in Gd_2O_2S samples doped with different Er^{3+} concentrations, [Er^{3+}], derived from the fitting of the decay curves using the four-level system presented in Figure 4 and Equation (1). See also text.

[Er^{3+}]	$W_{ETU}N_{10}$ [s^{-1}]	$W_{ETU}N_{10}$/[Er^{3+}]
0.1%	270	2700
2%	65	32
10%	220	22
15%	685	45
25%	3100	125

for k_{if} and thus the product $W_{ETU}N_{10}$ was the only free parameter. The $W_{ETU}N_{10}$ values obtained for different Er^{3+} concentrations are summarized in **Table 2**. The ratio between the energy transfer rate and the Er^{3+} concentration, $W_{ETU}N_{10}$/[Er^{3+}], is also given for comparison. The values estimated for the Gd_2O_2S samples doped with 2% Er^{3+}, 10% Er^{3+}, and 15% Er^{3+} correspond to increasing N_{10} with a same-order of magnitude W_{ETU} value. This result indicates that analogous energy transfer processes, with similar average distance between Er^{3+} ions, are responsible for the UC emission in these samples. Similarly to the excitation power dependent experiments (see previous section), the effect of increasing Er^{3+} concentration is an increase of the initial population of the $^4I_{13/2}$ intermediate state, N_{10}. The results for the samples doped with 0.1% Er^{3+} and 25% Er^{3+} show a strong deviation and the energy transfer rate, $W_{ETU}N_{10}$, in Gd_2O_2S:0.1%Er^{3+} is larger than the one expected if the same average distance as in the Gd_2O_2S samples doped with 2% Er^{3+}, 10% Er^{3+}, and 15% Er^{3+} is considered. As discussed before, in the diluted sample (0.1% Er^{3+}) energy migration is almost absent. As a result, the UC emission is only due to close-neighbor Er^{3+} ions, while pairs with a larger separation do not contribute to the UC luminescence. Hence, we observe a higher apparent energy transfer parameter, W_{ETU}. In the sample doped with 25% Er^{3+}, the energy transfer parameter is also unexpectedly large. We ascribe this to quenching processes by energy migration to quenching centers which depopulates the intermediate $^4I_{13/2}$ state. In our simple model the faster decay due to this additional quenching process appears as a larger fitted value for W_{ETU}. This result is in line with a shorter average distance between Er^{3+} ions for the sample doped with 25% Er^{3+}.

We further note that the decay time (see Table 1) slightly increases with Er^{3+} concentration up to the optimum Er^{3+} concentration (10%). An increase of the emission lifetime of different lanthanides when increasing the concentration was previously described for Y_2O_3 doped with Yb^{3+}, Er^{3+}, or Ho^{3+}, below the optimum concentration.[31,32] The lengthening of the lifetime was ascribed to reabsorption of the emitted radiation.[31,33] The decay time decreases for Er^{3+} concentrations higher than 10%. The decrease of the decay time above 10% Er^{3+}, which is accompanied by a reduction of the UC luminescence intensity (see Figure 1a), can be accounted for by concentration quenching due to cross-relaxation processes or energy migration to lattice defects. Similarly, a decrease of the lifetime above an optimum concentration is commonly observed, e.g., in Er^{3+}, Yb^{3+}, and Ho^{3+} doped Y_2O_3.[31,33]

Table 3. Lifetimes obtained for $^4I_{11/2}$ and $^4I_{13/2}$ emission in Er^{3+}-doped Gd_2O_2S for different Er^{3+} concentrations upon direct excitation in the emitting level, for undiluted microcrystalline powder and for the powder diluted in microcrystalline $BaSO_4$ powder (4 wt% Gd_2O_2S:Er^{3+}).

$^4I_{11/2}$	Powder τ [ms]	Diluted in $BaSO_4$ τ [ms]
0.1%	2.1 ± 0.1	2.0 ± 0.1
2%	4.3 ± 0.1	2.0 ± 0.1
10%	3.6 ± 0.1	2.0 ± 0.1
$^4I_{13/2}$		
0.1%	3.2 ± 0.1	2.8 ± 0.1
2%	5.1 ± 0.1	2.8 ± 0.1
	23.5 ± 0.5	
10%	3.7 ± 0.1	2.5 ± 0.1
	11.2 ± 0.2	

The concentration dependence of the luminescence decay time is consequence of two contributing effects, namely reabsorption of the UC emission intensity (giving rise to lengthening of the observed decay time) and nonradiative quenching (shortening the lifetime). To understand how the lengthening of the UC decay time up to 10% Er^{3+} is related to reabsorption and quenching processes, we determined the *direct* lifetimes of both $^4I_{13/2}$ and $^4I_{11/2}$ states in Gd_2O_2S doped with 0.1%, 2%, and 10% Er^{3+}.[31,33] We also compared these values to the *direct* lifetimes of the $^4I_{13/2}$ and $^4I_{11/2}$ states in Er^{3+}-doped Gd_2O_2S samples diluted to 4% (w/w) in microcrystalline $BaSO_4$ powder, where reabsorption is expected to be suppressed.[31]

Table 3 summarizes the lifetimes measured for the $^4I_{11/2}$ and $^4I_{13/2}$ emission in pure Gd_2O_2S:Er^{3+} and in Gd_2O_2S:Er^{3+} diluted with $BaSO_4$. We observe that in the undiluted Gd_2O_2S powder, the lifetimes for 2% and 10% Er^{3+} are significantly longer than for 0.1% Er^{3+}. The difference for the 2% Er^{3+}-doped sample is a factor ≈2 for the $^4I_{13/2}$ state and ≈1.5 for the $^4I_{11/2}$ state. This effect is a direct result of reabsorption. Indeed, it is not observed in the diluted samples, where reabsorption is strongly suppressed. We further note that for these samples the lifetimes for 10% Er^{3+} are slightly shorter than for 2% Er^{3+}. We ascribe this to the onset of concentration quenching effects.

Figure 10 illustrates that reabsorption affects not only lifetimes under direct excitation but also the UC dynamics and compares the $^4I_{11/2}$ UC emission decay curves in Gd_2O_2S:2%Er^{3+} both as pure powder and embedded in $BaSO_4$. No difference was noticed for the rise time, while the decay time of the Gd_2O_2S:2%Er^{3+} sample embedded in $BaSO_4$ is clearly shorter than the one of the Gd_2O_2S:2%Er^{3+} undiluted powder.

The optimum Er^{3+} concentration and UC quantum yield are not material properties. The UC efficiency varies between different sources for the material and can be linked to the quality of the samples. Systematic studies to explain the effects are scarce but generally differences in quantum yields for luminescent materials with the same nominal composition are explained by the presence of quenching centers (often assumed to be defects or impurities). For example, ppm levels of Fe^{3+} have been shown to quench luminescence in commercial lamp phosphors.[34] Higher quality samples provide lower quenching

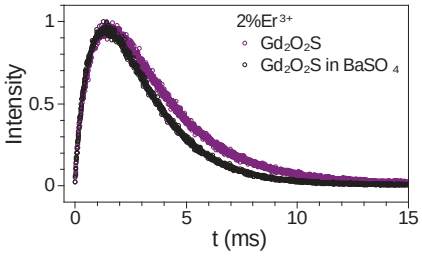

Figure 10. Temporal evolution of the $^4I_{11/2}$ UC emission in undiluted and diluted (in $BaSO_4$, to reduce reabsorption effects) Gd_2O_2S:2%Er^{3+} upon pulsed excitation at 1510 nm.

probability, and therefore show higher quantum yields and higher optimum concentrations. In addition, we have demonstrated that Gd_2O_2S:Er^{3+} presents higher energy transfer probability and lower optimum concentration than $NaYF_4$:Er^{3+}. Both features are directly related to the higher oscillator strengths for transitions in Er^{3+} in the Gd_2O_2S host lattice. However, it is worth noting that for higher oscillator strength the energy migration probability, and therefore the probability of quenching by energy transfer to defects also increases. Thus, interestingly, a host material with higher oscillator strength such as Gd_2O_2S is more suitable for UC applications (higher quantum yield), but also more vulnerable to defects, and therefore more difficult to optimize.

As mentioned above, only limited attention has been paid to the role of nondesired impurities or defects. As a final experiment, we demonstrate the importance of the sample quality to obtain a high UC efficiency. To understand the influence of defects on the luminescence quenching of the Er^{3+}-doped Gd_2O_2S UC material, we analyzed the optical properties of two different Gd_2O_2S samples doped with the same Er^{3+} concentration (10%). **Figure 11** compares the UC emission intensity and lifetime of the optimized Gd_2O_2S:10%Er^{3+} UC material studied in the present work to a Gd_2O_2S:10%Er^{3+} sample obtained from a different supplier (the so-called *test* sample, obtained from Tailorlux GmbH). From inductively coupled plasma (ICP) measurements the Er^{3+} concentration was estimated to be 10.5% ± 0.5% for both samples. The synthesis procedure influences the quality of the UC material, which is a key parameter to obtain highly efficient luminescent materials. As it can be seen in Figure 11a, the two nominally identical samples exhibit a factor of four difference in the UC emission intensity. The lower intensity is accompanied by a shorter UC lifetime (see Figure 11b). Hence, we ascribe the reduction of the UC luminescence intensity to energy transfer to quenching centers. Assuming homogeneous Er^{3+} distribution in both samples (equal probability for cross-relaxation processes), the reduced intensity in the *test* sample is due to energy migration of the excitation to defects or impurities in the host lattice. Thus, the results in Figure 11 illustrate the important role of defects and impurities on the UC efficiency, although the precise nature of the defects and impurities is difficult to elucidate.

3. Conclusion

Detailed spectroscopic studies have provided a better understanding of the UC processes in the highly efficient UC material Gd_2O_2S:Er^{3+}. Analysis of the excitation and emission spectra and time resolved UC emission spectroscopy reveal that the ($^4I_{13/2}$, $^4I_{13/2}$) → ($^4I_{15/2}$, $^4I_{9/2}$) ETU mechanism is responsible for the $^4I_{9/2}$ (820 nm) and $^4I_{11/2}$ (1000 nm) UC luminescence in Er^{3+}-doped Gd_2O_2S, even at Er^{3+} concentrations as low as 0.1%. The temporal evolution of the UC emission after pulsed excitation was analyzed using a rate equation model. The modeling provides a good agreement with experimental results. It reproduces the fast rise time of the $^4I_{9/2}$ UC emission, determined by the fast decay of the intermediate $^4I_{9/2}$ state. Power dependent UC emission decay curves demonstrate a faster UC rise time for higher excitation densities, analogous to previous observations for organic UC materials relying on triplet–triplet annihilation. Modeling UC emission decay curves for different excitation powers, extending into the saturation regime, allows for the determination of the UC energy transfer parameter W_{ETU} at 6.3×10^{-19} cm^3 s^{-1}. This parameter is a measure of the ETU efficiency and can be compared between different UC materials. A similar analysis for the $NaYF_4$:Er^{3+} UC material shows that W_{ETU} is about ten times smaller in this material. Concentration dependent results demonstrate that the ultimate UC efficiency depends not only on W_{ETU} but also on an interplay among diverse phenomena such as radiative decay, energy transfer and migration, reabsorption and quenching centers

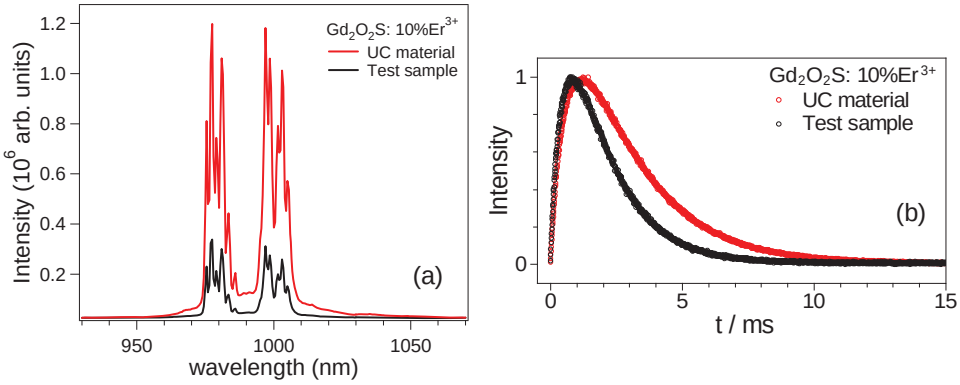

Figure 11. a) $^4I_{11/2}$ UC emission spectra and b) lifetime of Gd_2O_2S doped with 10%Er^{3+}. The efficient material studied in this work (red) is compared to a test sample (black) with the same composition.

(defects and impurities). The insights obtained will contribute to the development of optimized UC materials and aid in determining the ultimate limit of the UC efficiency that can be realized in a material where luminescence quenching is completely suppressed.

4. Experimental Section

Er^{3+}-doped Gd_2O_2S microcrystalline samples (different Er^{3+} concentrations) were custom made for our research purposes by Leuchtstoffwerk Breitungen GmbH (Breitungen, Germany), which has optimized the synthesis of lanthanide-doped Gd_2O_2S for X-ray diagnostics. For comparison purposes, another Gd_2O_2S:10%Er^{3+} sample (the so called *test* sample) was obtained from Tailorlux GmbH (Münster, Germany). The efficient $NaYF_4$:25%Er^{3+} microcrystalline sample synthesized in K.W. Krämer group (University of Bern) was also studied. Er^{3+} concentrations were determined by ICP atomic emission spectroscopy. Room temperature UC emission, excitation, and luminescence decay measurements were performed using an optical parametric oscillator (OPO) system (Opotek HE 355 II) pumped by the third harmonic of a Nd:YAG laser (Nd^{3+}-doped yttrium aluminium garnet) as excitation source. This OPO system offers a continuous tunable optical range from 410 to 2400 nm, with Gaussian beam profile, a maximum energy of 2 mJ per pulse in the infrared range, a pulse width of 10 ns, and a repetition rate of 20 Hz. Unless otherwise stated, spectra and decay curves were obtained upon pulsed-excitation into the $^4I_{13/2}$ state at 1510 nm. The N_2-cooled R5509-72 photomultiplier tube detector of the spectrofluorometer (Edinburgh Instruments FLS 920) was used for detection in the infrared range. Excitation spectra were recorded with a gated photon counter (Stanford Research Systems SR400), with typical gate width of 10 ms and a delay of 0.2 μs. Power-dependent luminescence decay measurements were carried out upon excitation with the OPO system combined with different calibrated neutral density filters. The OPO output energy was measured with a pyroelectric sensor (Coherent J-50MB-LE) controlled by a FieldMaxII-TOP energy- and power-meter. The excitation power density was calculated by considering the 10 ns pulse width and 3 mm spot diameter of the OPO beam.

Acknowledgements

The authors are grateful to Dr. Karl W. Krämer for providing high-quality $NaYF_4$:25%Er^{3+} microcrystalline samples. Financial support from the EU-FP7 NanoSpec programme (NMP-2009-246200) is also gratefully acknowledged.

Received: December 8, 2014
Revised: January 7, 2015
Published online: February 3, 2015

[1] F. Auzel, *Acad. Sci.* **1966**, *262*, 1016.
[2] V. V. Ovsyankin, P. P. Feofilov, *JETP Lett.* **1966**, *3*, 322.
[3] M. Nyk, R. Kumar, T. Y. Ohulchanskyy, E. J. Bergey, P. N. Prasad, *Nano Lett.* **2008**, *8*, 3834.
[4] T. Trupke, A. Shalav, B. S. Richards, P. Würfel, M. A. Green, *Sol. Energy Mater. Sol. Cells* **2006**, *90*, 3327.
[5] J. C. Goldschmidt, S. Fischer, P. Löper, K. Krämer, D. Biner, M. Hermle, S. W. Glunz, *Sol. Energy Mater. Sol. Cells* **2011**, *95*, 1960.
[6] H. Wang, M. Xing, X. Luo, X. Zhou, Y. Fu, T. Jiang, Y. Peng, Y. Ma, X. Duan, *J. Alloys Compd.* **2014**, *587*, 344.
[7] S. Han, R. Deng, X. Xie, X. Liu, *Angew. Chem. Int. Ed.* **2014**, *53*, 11702.
[8] T. Trupke, M. A. Green, P. Würfel, *J. Appl. Phys.* **2002**, *92*(7), 4117.
[9] A. Shalav, B. S. Richards, T. Trupke, K. W. Krämer, H. U. Güdel, *Appl. Phys. Lett.* **2010**, *108*, 044912.
[10] F. Auzel, *Chem. Rev.* **2004**, *104*, 139.
[11] H. U. Güdel, M. Pollnau, *J. Alloys Compd.* **2000**, *303–304*, 307.
[12] A. Shalav, B. S. Richards, T. Trupke, K. W. Krämer, H. U. Güdel, *Appl. Phys. Lett.* **2005**, *86*, 013505.
[13] G. Chen, T. Y. Ohulchanskyy, A. Kachynski, H. Agren, P. N. Prasad, *ACS Nano* **2011**, *5*, 4981.
[14] G. A. Kumar, M. Pokhrel, D. K. Sardar, *Mater. Lett.* **2012**, *68*, 395.
[15] D. R. Gamelin, H. U. Güdel, in *Topics in Current Chemsitry*, Vol. *214*, Springer-Verlag, Berlin **2001**.
[16] T. Förster, *Ann. Phys.* **1948**, *2*, 55.
[17] L. Agazzi, K. Wörhoff, M. Pollnau, *J. Phys. Chem. C* **2013**, *117*, 6759.
[18] S. Fischer, B. Fröhlich, H. Steinkemper, K. W. Krämer, J. C. Goldschmidt, *Sol. Energy Mater. Sol. Cells* **2014**, *122*, 197.
[19] R. Martín-Rodríguez, S. Fischer, A. Ivaturi, B. Froehlich, K. W. Krämer, J. C. Goldschmidt, B. S. Richards, A. Meijerink, *Chem. Mater.* **2013**, *25*, 1912.
[20] M. Pollnau, D. R. Gamelin, S. R. Lüthi, H. U. Güdel, *Phys. Rev. B* **2000**, *61*, 3337.
[21] J. F. Suyver, A. Aebischer, S. García-Revilla, P. Gerner, H. U. Güdel, *Phys. Rev. B* **2005**, *71*, 125123.
[22] S. Baluschev, T. Miteva, V. Yakutkin, G. Nelles, A. Yasuda, G. Wegner, *Phys. Rev. Lett.* **2006**, *97*, 143903.
[23] S. Baluschev, V. Yakutkin, T. Miteva, G. Wegner, T. Roberts, G. Nelles, A. Yasuda, S. Chernov, S. Aleshchenkov, A. Cheprakov, *New J. Phys.* **2008**, *10*, 013007.
[24] A. Shalav, B. S. Richards, K. Krämer, G. Conibeer, M. A. Green, *Proc. WCPEC-4 1* **2007**, *45*, 4059557.
[25] D. R. Gamelin, H. U. Güdel, *J. Phys. Chem. B* **2000**, *104*, 10222.
[26] Y. Guyot, H. Manaa, J. Y. Rivoire, R. Moncorgé, N. Garnier, E. Descroix, M. Bon, P. Laporte, *Phys. Rev. B* **1995**, *51*, 784.
[27] R. Buisson, J. C. Vial, *J. Physique Lett.* **1981**, *42*, 115.
[28] D. R. Gamelin, H. U. Güdel, *Inorg. Chem.* **1999**, *38*, 5154.
[29] M. Pollnau, P. J. Hardman, W. A. Clarkson, D. C. Hanna, *Opt. Commun.* **1998**, *147*, 203.
[30] D. J. Simkin, J. A. Koningstein, P. Mysiinski, S. A. Boothroyd, J. Chrostowski, *J. Appl. Phys.* **1993**, *73*, 8046.
[31] F. Auzel, G. Baldacchini, L. Laversenne, G. Boulon, *Opt. Mater.* **2003**, *24*, 103.
[32] L. Laversenne, Y. Guyot, C. Goutadier, M. T. Cohen-Addad, G. Boulon, *Opt. Mater.* **2001**, *16*, 475.
[33] F. Auzel, F. Bonfigli, S. Gagliari, G. Baldacchini, *J. Lumin.* **2001**, *94*, 293.
[34] W. van Schaik, S. Lizzo, W. Smit, G. Blasse, *J. Electrochem. Soc.* **1993**, *140*, 216.